Author(s): Peuronen, Anssi; Kivelä, Henri; Salonen, Pasi; Eskonen, Ville; Karman, Marta; Lahtinen, Manu; Romanowski, Grzegorz; Lehtonen, Ari

Title: Molybdenum(VI) complexes with a chiral L-alanine bisphenol [O,N,O,O'] ligand : Synthesis, structure, spectroscopic properties and catalytic activity

Year: 2023

Version: Published version

Inorganica Chimica Acta 553 (2023) 121519

Contents lists available at ScienceDirect

Inorganica Chimica Acta

journal homepage: www.elsevier.com/locate/ica

Molybdenum(VI) complexes with a chiral L-alanine bisphenol [O,N,O,O'] ligand. Synthesis, structure, spectroscopic properties and catalytic activity

Anssi Peuronen [a,b], Henri Kivelä [a], Pasi Salonen [a], Ville Eskonen [a], Marta Karman [c], Manu Lahtinen [b], Grzegorz Romanowski [c], Ari Lehtonen [a,*]

[a] Department of Chemistry, University of Turku, FI-20014 Turku, Finland
[b] Department of Chemistry, University of Jyväskylä, P.O. Box 35, FI-40014 JY, Finland
[c] Faculty of Chemistry, University of Gdańsk, Wita Stwosza 63, PL-80308 Gdańsk, Poland

ARTICLE INFO

Keywords:
Molybdenum
L-alanine
Epoxidations
Catalysis

ABSTRACT

Dioxidomolybdenum(VI) compound $[MoO_2Cl_2(dmso)_2]$ reacts with a chiral tetradentate O_3N-type L-alanine bisphenol ligand precursor $(Et_3NH)H_2L^{ala}$ to form an oxidochloridomolybdenum(VI) complex $[MoOCl(L^{ala})]$ (**1**) as two separable geometric isomers with phenolate groups in *cis* or *trans* positions. The single crystal X-ray and NMR analyses of *cis*- and *trans*-**1** reveal that the complexes are formed of monomeric molecules, in which the ligand has a tetradentate coordination through three oxygen donors and one nitrogen donor. The reaction of $Na_2MoO_4{\cdot}2H_2O$ with the same ligand precursor in an acidic methanol solution leads to the formation of an anionic dioxido complex $(Et_3NH)[MoO_2(L^{ala})]$ (**2**) with a *trans* coordination of the tetradentate ligand. *Trans*-**1** and **2** were studied as active catalysts for olefin epoxidation: *i.e.* styrene, cyclohexene, *S*(–)-limonene and (–)-α-pinene using H_2O_2 and tBuOOH as oxidants.

1. Introduction

In transition metal chemistry, diverse ligands are utilized to modify the surroundings of the metal. Especially, the reactivity of the metal species is substantially dependent on the steric properties of the ligands, whereas a number of bulky anionic ligands with hard oxygen donor atoms have been used to get robust complexes which are stable under ambient conditions. To this end, several phenolato ligands, particularly, have shown great potential [1–3]. For example, amine bisphenols with various donors in the pendant arm form a family of readily available and adjustable tetradentate ligands, which can form chelates through hard nitrogen and oxygen donor atoms. They are combined with metals from across the periodic table to form molecular complexes, which can be used e.g. as active catalysts for a number of reactions [4]. The research on the coordination chemistry of molybdenum is often inspired by its role in several biological oxidation and oxotransfer (OAT) reactions [5]. As a result, a number of molybdenum-containing model compounds for OAT reactions have been studied [6–9]. Similarly, a number of artificial dioxidomolybdenum(VI) compounds have been used in important industrial processes, such as olefin epoxidation [10–12]. Generally, the molybdenum catalysts involve metal ions in high oxidation states, and thus the reactivity of many active species can be modelled with isolated oxidomolybdenum species, whereas such model compounds are commonly prepared using multidentate phenolato ligands. For example, the reactions of MoO_2Cl_2 and its soluble derivatives with amine trisphenols, aminoalcohol bisphenols or aminoacid bisphenols are known to yield neutral, mononuclear oxidochloridomolybdenum(VI) [MoOCl(L)] type complexes which can catalyze various oxidation reactions, for instance sulfoxidation, epoxidation and haloperoxidation [13–15]. A tetrapodal ligand can coordinate to the metal center in a fashion resembling a three-bladed propeller, which generates a chiral environment around the metal. This, however, typically leads to the formation of two enantiomers instead of enantiopure products. When introducing a ligand-based chirality to the metal complexes, natural α-amino acids are useful building blocks for the preparation of enantiopure ligands.

As epoxides are valuable precursors for a wide variety of organic functionalities in the synthesis of fine chemicals and pharmaceutical intermediates, the catalytic oxidation of alkenes is one of the most extensively studied reactions in organic chemistry [16,17]. Furthermore, transformation of epoxides is also a key step for numerous processes important for both synthetic organic chemistry and biochemistry, due to the ring-opening reaction of epoxides generating new useful

* Corresponding author.
E-mail address: ari.lehtonen@utu.fi (A. Lehtonen).

https://doi.org/10.1016/j.ica.2023.121519
Received 16 February 2023; Received in revised form 5 April 2023; Accepted 6 April 2023
Available online 7 April 2023

carbon–carbon bonds [18,19]. From the industrial point of view, there is an interest on some plant-derived monoterpenes which can be accumulated in bulk amounts from biogenic waste streams. Particular attention has recently been paid on monocyclic and bicyclic monoterpenes, such as abundant natural products limonene and pinene, but also on inexpensive by-products from technical forestry resins and wood pulp by-produced in the cellulose manufacture [20] and the citrus fruit juice industry [21], respectively.

Although *R*(+)-limonene is the primary enantiomer in most plants that produce limonene, the resin from a few plants such as *Pinus strobus* L. contains substantial amounts of the *S*(–)-enantiomer, as well. α-Pinene is the major monoterpene of pine essential oils widely used as a food flavoring ingredient and also accepted as a safe food additive [22]. In recent years, there has been a growing interest in the synthesis of their oxidation products especially optically pure epoxides which have been found as important building blocks in asymmetric synthesis and are more particularly used as chiral precursors [23].

In this study, we used an amine bisphenol derivative of L-alanine ($(Et_3NH)H_2L^{ala}$) to prepare new oxidomolybdenum(VI) complexes with a chiral chelating ligand. The epoxidation activities for styrene, cyclohexene, *S*(–)-limonene and (–)-α-pinene were tested using H_2O_2 and tBuOOH as oxidants.

2. Experimental

2.1. General remarks

The ligand precursor $(Et_3NH)H_2L^{ala}$ was made of L-alanine, 2–4-di-*tert*-butylphenol, paraformaldehyde and triethylamine using the known procedures. [24,25]. $MoO_2Cl_2(dmso)_2$ was prepared following the published method [26]. Other chemicals and solvents were obtained from commercial sources and were used as purchased. All syntheses were carried out under ambient atmosphere. The IR spectra were measured with Bruker Optics, Vertex 70 device with a diamond ATR setup. The UV spectra were recorded in $CHCl_3$ solutions. A Shimadzu GC-2025 gas chromatograph with a Zebron ZB-5 capillary column (30 m × 0.25 mm × 0.25 mm) and FID detector were used to analyse the reaction products of the oxidation of olefins. The identity of the products was confirmed using a GC–MS model Shimadzu GCMS-QP2010 SE. Single crystal X-ray data were collected by Rigaku Oxford Diffraction SuperNova diffractometer equipped with micro-focus dual-source (Mo/Cu) and Atlas detector using Cu K_α (λ = 1.54184) radiation. The crystals were kept under a nitrogen stream at 123 K during data collection. Data collection and reduction were carried out in CrysAlis^{Pro} software whereas Olex^2 GUI was used for crystal structure solving (SHELXS) and refinement (SHELXL). For *cis*-**1** and *trans*-**1** all non-hydrogen atoms were located from the difference density map and refined using anisotropic displacement parameters whereas a standard SHELXL riding atom model was used for hydrogen atoms. Disorder is observed for crystal structures of both *cis*-**1** and *trans*-**1**. For *cis*-**1**, which crystallised as an acetonitrile solvate, one of the two acetonitrile molecules in the asymmetric unit was refined with two positions with ca. 0.7:0.3 occupancies. In case of *trans*-**1**, one of the two distinct complex molecules in the asymmetric unit shows disorder of one of the four *tert*-butyl groups (central carbon C25B). Consequently, the *tert*-butyl group was refined with two distinct positions with ca. 0.83:0.17 occupancies while the C—C distances and anisotropic parameters were restrained using SADI and SIMU. CheckCIF/PLATON procedure finds a potential higher symmetry for *trans*-**1** (space group $P2_1/c$). The data could be solved and refined in this centrosymmetric space group, but resulted in a disagreeably high *R*-values as well as disorder of the L-alanine moiety suggesting that the initial space group $P2_1$ is correctly assigned and no racemisation of the chiral centre has occurred during the synthesis. The crystal structure of **2** was solved in space group *P*1 and only partially refined to determine the molecular geometry and conformation of the complex (see further details in ESI).

2.2. NMR spectroscopy

The ^1H and ^{13}C NMR spectra were measured with a 500 MHz Bruker Avance (^1H: 500.13 MHz, ^{13}C: 125.76 MHz) or Avance III (^1H: 500.08 MHz, ^{13}C: 125.75 MHz) spectrometer. Deuterated chloroform ($CDCl_3$) at 25 °C was used as solvent for *cis*- and *trans*-**1**, and DMSO-d_6 at 30 °C for **2**. Proton and carbon chemical shifts were referenced to internal tetramethylsilane ($\delta_{TMS} = 0.00$ ppm). The 1D ^1H NMR spectra were measured with a single-pulse-acquire sequence (Bruker pulse program "zg30") with a 30° flip angle and a 4.3–5.1 s recycle delay. For the 1D ^{13}C NMR spectra ("zgpg30"), a 30° flip angle, 3.1 s recycle delay, and broadband ^1H decoupling ("waltz16") were used. The gradient-selected ^1H–^1H COSY spectra were recorded in a double-quantum filtered mode ("cosygpmfqf"). ^1H–^1H NOE spectra were acquired with 1D ("selnogp") and 2D ("NOEsygpph") transient NOESY experiments using a 0.30 s mixing time. The ^1H–^{13}C HSQC spectra ("hsqcedetgpsisp2") were recorded with multiplicity editing (resulting in positive CH, CH_3 and negative CH_2 correlation signals) and were optimized for a 145 Hz one-bond ^1H–^{13}C coupling constant. The ^1H–^{13}C HMBC long-range correlation experiments ("hmbcgplpndqf") were optimized for a 10 Hz (long-range) ^1H–^{13}C coupling constant while utilizing a 145 Hz low-pass *J*-filter. The dynamic lineshape analyses were done with the DNMR Lineshape Analysis module ver. 1.1 included in Bruker's TopSpin 4.0.2 software.

2.3. Computational chemistry

The molecular model building and basic molecular mechanics (MM) geometry optimizations were done with the ChemDraw 20.0 and Chem3D 20.0 software, using the MM2 force field. For MM-based conformational search for complex **2**, Materials Studio Conformers simulation tool included in the BIOVIA Materials Studio environment was used. The DFT geometry optimizations and GIAO NMR chemical shift calculations were done with Gaussian 09 or Gaussian 16 software [27] using the B3LYP functional and an atom-specific basis set with def2-TZVP and effective core potential (ECP) for Mo and 6–31 + G(d,p) for the other atoms. The chemical shifts were calculated for the DFT-optimized structures both in a gas phase and in solution, with the PCM method used to model the chloroform (for *cis*-**1** and *trans*-**1**) and DMSO (for **2**) solvents. The Cartesian coordinates of the DFT-optimized geometries of *cis*-**1**, *trans*-**1**, *trans*-**2**-A and *trans*-**2**-B are given in ESI Table S1.

2.4. Molybdenum(VI) complexes

2.4.1. Synthesis of 1

1.0 mmol batches of $[Et_3NH]H_2L^{ala}$ (0.63 g) and $MoO_2Cl_2(dmso)_2$ (0.36 g) were mixed with 40 ml of toluene and the reaction mixture was refluxed for 6 h. Blue *trans*-**1** and purple *cis*-**1** were isolated from the reaction mixture by silica column chromatography using CH_2Cl_2 as an eluent. The synthesis was repeated several times, while the yields for *trans*-**1** were typically 50–70% and for *cis*-**1** the yields were 5–10 %. Small amounts of **2** were isolated from the reaction mixture by adding 2% of Et_3N in the eluent. Crystals of *cis*-**1** and *trans*-**1** for X-ray studies were obtained from hot acetonitrile upon cooling to room temperature.

Cis-**1**: IR: 2961 s, 2930 m, 2861 m, 1718 vs, 1593 s, 1458 s, 1393 w, 1381 m, 1360 m, 1310 m, 1283 w, 1257 w, 1240 s, 1200 s, 1169 vs, 1114 m, 1066 m, 1025 w, 1008 w, 961 vs, 953 vs, 940 m, 929 w, 914 s, 879 vs, 869 vs, 847 s, 826 m, 808 s, 761 m, 752 m, 704 m, 654 w cm^{-1}. UV: ε 4450 (320 nm), 6080 (503 nm), 9010 (685 nm) $dm^3mol^{-1}cm^{-1}$. ^1H NMR ($CDCl_3$): δ 7.42 (2H, m, 3-H & 13-H), 7.22 (1H, d, $J = 2.2$ Hz, 11-H), 7.16 (1H, d, $J = 2.1$ Hz, 5-H), 4.79 (1H, d, $J = 13.8$ Hz, 7-H_{syn}), 4.01 (1H, quartet, $J = 7.0$ Hz, 16-H), 3.73 (1H, d, $J = 13.8$ Hz, 7-H_{anti}), 3.57 (1H, d, $J = 13.6$ Hz, 9-H_{syn}), 3.42 (1H, d, $J = 13.6$ Hz, 9-H_{anti}), 1.53 (9H, s, 2-*t*Bu), 1.51 (3H, d, $J = 7.0$ Hz, 16-CH_3), 1.47 (9H, s, 14-*t*Bu), 1.33 (9H, s, 4-*t*Bu), 1.29 (9H, s, 12-*t*Bu). ^{13}C NMR ($CDCl_3$): δ 172.5 (C17),

162.9 (C15), 157.1 (C1), 151.3 (C4), 149.4 (C12), 140.7 (*C*2), 140.4 (C14), 129.6 (C6), 129.1 (C10), 125.5 (C11), 125.4 (C5), 124.5 (C13), 124.1 (C3), 63.0 (C16), 60.7 (C7), 52.1 (C9), 35.8 (2-*C*$(CH_3)_3$), 35.2, 35.1 (4-*C*$(CH_3)_3$ & 14-*C*$(CH_3)_3$), 34.9 (12-*C*$(CH_3)_3$), 31.5 (12-C(*C*$H_3)_3$), 31.4 (4-C(*C*$H_3)_3$), 30.4 (2-C(*C*$H_3)_3$), 29.9 (14-C(*C*$H_3)_3$), 9.2 (16-*C*H_3).

Trans-**1**: IR: 2956 s, 2925 vs, 2856 s, 1690 vs, 1593 s, 1461 s, 1392 m, 1375 m, 1363 m, 1330 w, 1306 w, 1290 w, 1259 s, 1239 vs, 1201 s, 1169 vs, 1122 m, 1094 m, 1067 m, 1040 m, 1023 s, 953 vs, 917 s, 880 s, 862 vs, 807 s, 775 m, 757 s, 695 m, 657 w cm^{-1}. UV: ε 1580 (365 nm), 4940 (515 nm), 13,800 (683 nm) $dm^3mol^{-1}cm^{-1}$. ^{1}H NMR ($CDCl_3$): δ 7.44 (2H, m, 3-H & 13-H), 7.15 (1H, d, *J* = 2.2 Hz, 11-H), 7.08 (1H, d, *J* = 2.1 Hz, 5-H), 4.82 (1H, d, *J* = 14.4 Hz, 7-H_{anti}), 4.22 (1H, d, *J* = 13.6 Hz, 9-H_{anti}), 3.74 (2H, m, 7-H_{syn} & 9-H_{syn}), 3.57 (1H, quartet, *J* = 7.0 Hz, 16-H), 1.57 (9H, s, 14-*t*Bu), 1.54 (9H, s, 2-*t*Bu), 1.34 (9H, s, 4-*t*Bu), 1.33 (9H, s, 12-*t*Bu), 1.26 (3H, d, *J* = 7.0 Hz, 16-CH_3). ^{13}C NMR ($CDCl_3$): δ 173.7 (C17), 162.0 (C15), 159.9 (C1), 152.0 (C4), 151.0 (C12), 141.5 (*C*2), 139.7 (C14), 128.8 (C6), 127.5 (C10), 126.1 (C11), 125.8 (C5), 124.4 (C13), 124.2 (C3), 60.7 (C7), 58.7 (C16), 56.5 (C9), 35.7 (2-*C*$(CH_3)_3$), 35.5 (14-*C*$(CH_3)_3$), 35.2, 35.1 (4-*C*$(CH_3)_3$ & 12-*C*$(CH_3)_3$), 31.4, 31.4 (4-C(*C*$H_3)_3$ & 12-C(*C*$H_3)_3$), 30.3, 30.2 (2-C(*C*$H_3)_3$ & 14-C(*C*$H_3)_3$), 8.9 (16-*C*H_3).

2.4.2. Synthesis of 2

0.50 mmol of $Na_2MoO_4{\cdot}2H_2O$ (0.19 g) was mixed with a 0.43 mmol of $(Et_3NH)(H_2L^{ala})$ (0.27 g) in 10 ml of MeOH. Acetic acid (0.1 ml) was added and the reaction mixture was heated to the reflux temperature for two hours, cooled to the room temperature and stored at + 4 °C overnight to obtain 200 mg (62 %) of an orange-yellow solid product. IR: 3090 m(br), 3000 m, 2955 m, 2900 m, 2864 m, 1670 s, 1580 m, 1470 s, 1440 m, 1412 m, 1380 m, 1361 m, 1330 m, 1305 w, 1275 m, 1255 s, 1237 vs, 1203 m, 1168 s, 1120 m, 1079 m, 1041 w, 1009 m, 979 w, 920 s, 885 vs, 840 s, 821 s, 806 m, 776 m, 759 m, 740 m, 698 w, 674 w, 649 w, 622 m, 601 m, 550 s cm^{-1}. ^{1}H NMR (DMSO-d_6): δ 8.88 (1H, br s, N*H*$(CH_2CH_3)_3$), 7.13 (1H, d, *J* = 2.4 Hz, 13-H), 7.05 (1H, d, *J* = 2.3 Hz, 11-H), 7.03 (1H, d, *J* = 2.3 Hz, 3-H), 6.90 (1H, d, *J* = 2.3 Hz, 5-H), 4.77 (1H, d, *J* = 15.1 Hz, 7-H_{anti}), 3.81 (1H, d, *J* = 15.1 Hz, 7-H_{syn}), 3.63 (1H, br d, 9-H_{anti}), 3.48 (1H, d, *J* = 12.3 Hz, 9-H_{syn}), 3.29 (1H, under the H_2O peak, 16-H), 3.08 (6H, quartet, *J* = 7.3 Hz, NH(C$H_2$$CH_3)_3$), 1.35 (9H, s, 14-*t*Bu), 1.28 (9H, s, 2-*t*Bu), 1.25 (9H, s, 12-*t*Bu), 1.23 (9H, s, 4-*t*Bu), 1.17 (9H, t, *J* = 7.3 Hz, NH(CH_2C$H_3)_3$), 1.13 (3H, d, *J* = 7.1 Hz, 16-CH_3). ^{13}C NMR (DMSO-d_6): δ 174.9 (br, C17), 162.2 (br, C15), 160.3 (C1), 139.7 (C4), 139.4 (br, C12), 136.5 (*C*2), 135.4 (br, C14), 124.8 (C11), 124.0 (br, C10), 123.2 (C5), 122.6 (C13), 122.1 (C6), 120.6 (C3), 58.3 (2C, br, C7 & C16), 54.9 (C9), 45.7 (NH(*C*$H_2CH_3)_3$), 34.6 (2-*C*$(CH_3)_3$), 34.2 (14-*C*$(CH_3)_3$), 33.7 (2C, 4-*C*$(CH_3)_3$ & 12-*C*$(CH_3)_3$), 31.5 (12-C(*C*$H_3)_3$), 31.4 (4-C(*C*$H_3)_3$), 29.9 (14-C(*C*$H_3)_3$), 29.6 (2-C(*C*$H_3)_3$), 8.6 (NH(CH_2*C*$H_3)_3$), 8.4 (16-*C*H_3).

2.5. Oxidation of olefins

In a typical procedure, styrene or cyclohexene (1.00 mmol), an oxidant (3.00 mmol), *i.e.* aqueous 30% H_2O_2 or 5.5 M of tBuOOH in decane, and catalyst (0.020 mmol) were heated at 80 °C for 1 h of reaction time in 10 ml of 1,2-dichloroethane (DCE). The reactions were monitored by GC and the yields were recorded as GC yield based on the starting styrene or cyclohexene. The oxidation products were characterized by GC–MS. The influence of amounts of catalyst and oxidant was also studied to check their effect on the conversion and selectivity of the reaction products.

3. Results and discussions

3.1. Syntheses.

The ligand $(Et_3NH)H_2L^{ala}$ was made of L-alanine, 2–4-di-*tert*-butylphenol, formaldehyde and triethylamine modifying slightly the known procedures [24,25]. The reaction of stoichiometric amounts of $MoO_2Cl_2(dmso)_2$ and $(Et_3NH)H_2L^{ala}$ in refluxing toluene leads to a dark solution, which contained blue *trans*-**1** as a major product and small amount of purple *cis*-**1** as well as a trace amount of a yellow product **2** (Scheme 1). The components were isolated by column chromatography and identified by IR and NMR spectroscopy. The molecular structures were also verified by single crystal X-ray diffraction (see below). The IR spectra of *cis*-**1** and *trans*-**1** show strong IR absorptions at 914 and 917 cm^{-1}, respectively, which can be assigned as Mo=O stretch, but they lack the typical doublets for the MoO_2 moiety. On the contrary, complex **2** show strong IR-absorptions at 920 and 885 cm^{-1} – characteristic for the octahedral complexes carrying a MoO_2 function [28]. The reaction was repeated several times by applying different concentrations and reaction times but only *trans*-**1** was obtained in practical yields whereas *cis*-**1** and **2** could be isolated only in minor quantities. In general, the shorter reaction times yielded larger relative ratio of *cis*-**1** even if the yields were lower, but *cis*-**1** tends to isomerize to *trans*-**1** upon purification steps. The yellow product **2** was prepared for the further analyses and catalyst tests in a higher yield by the reaction of $Na_2MoO_4{\cdot}2H_2O$ with $(Et_3NH)H_2L^{ala}$ in an acidic methanol solution (Scheme 1b).

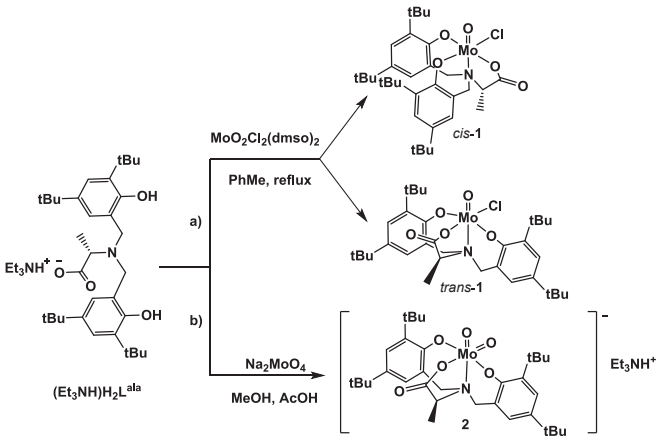

Scheme 1. Formation of the complexes *cis*-**1**, *trans*-**1** and **2** from L-alanine derived ligand precursor $(Et_3NH)H_2L^{ala}$.

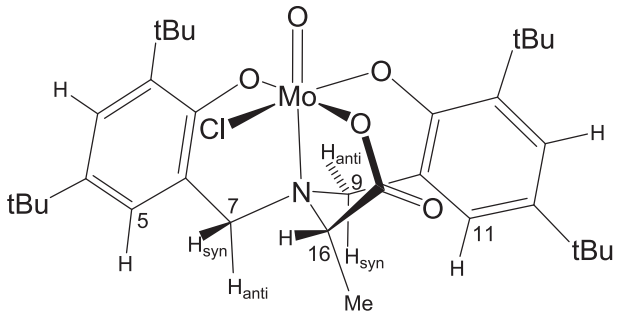

Fig. 1. Solution structure of *cis*-**1** in $CDCl_3$ as deduced by NMR spectroscopy. For clarity, the *t*Bu and Me groups have been contracted.

3.2. Solution structures.

The solution structures of the oxidochlorido complexes *cis*-**1** and *trans*-**1**, and the dioxido complex **2** were determined with 1D and 2D ^{1}H and ^{13}C NMR spectroscopy.

The ^{1}H and ^{13}C NMR spectra of *cis*- and *trans*-**1** dissolved in $CDCl_3$ feature sharp resonance peaks whose total number and intensities are consistent with the electrically neutral, diamagnetic, monomeric structures shown in Scheme 1. The NMR peaks were assigned, including stereochemistry of the diastereotopic geminal hydrogens, with help of

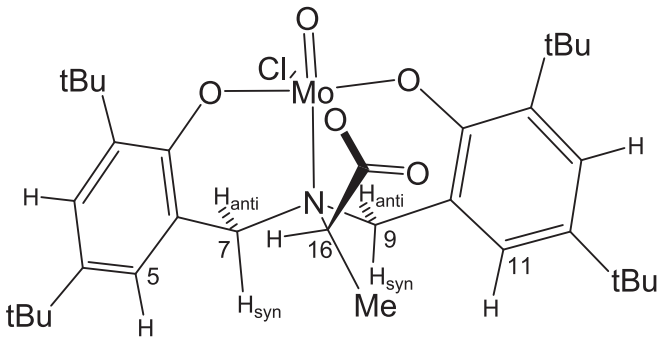

Fig. 2. Solution structure of *trans*-**1** in $CDCl_3$ as deduced by NMR spectroscopy.

Table 1
The chemical shifts δ (ppm) of selected protons of *cis*-**1**, *trans*-**1**, and **2**, and their relevant NOE and HMBC correlations. The atom numbering and the syn/anti descriptors are explained in the text and in Figs. 1 and 2.

Complex	proton	δ/ppm	NOE correlations	HMBC correlations[a]
cis-**1**	7-H_{syn}	4.79	16-H, 7-H_{anti}	C9
	16-H	4.01	7-H_{syn}, 16-Me	C9
	7-H_{anti}	3.73	5-H, 7-H_{syn}, 9-H_{syn}, 16-Me	–
	9-H_{syn}	3.57	11-H, 7-H_{anti}, 9-H_{anti}, 16-Me	–
	9-H_{anti}	3.42	9-H_{syn}	C16
	16-Me[b]	1.51	11-H, 16-H, 7-H_{anti}, 9-H_{syn}	C16
trans-**1**	7-H_{anti}	4.82	9-H_{anti}, 7-H_{syn}	C16
	9-H_{anti}	4.22	7-H_{anti}, 9-H_{syn}	C16
	7-H_{syn}[b]	3.745	5-H, 7-H_{anti}, 16-H, 16-Me	–
	9-H_{syn}[b]	3.739	11-H, 9-H_{anti}, 16-Me	–
	16-H	3.57	7-H_{syn}, 16-Me	C9
	16-Me	1.26	11-H, 7-H_{syn}, 9-H_{syn}	C16
(*trans*-) **2**	7-H_{anti}	4.77	7-H_{syn}	C16
	7-H_{syn}	3.81	7-H_{anti}, 16-H(w), 16-Me	C9, C16(w)
	9-H_{anti}	3.63 (br)	n.d.[c]	n.d.[c]
	9-H_{syn}[b]	3.48		C7/C16
	16-H[b]	3.29		C9
	16-Me	1.13	11-H, 7-H_{syn}, 9-H_{syn}, 16-H	C16

[a] HMBC (opt. for $^{n}J_{CH} = 10$ Hz) correlations from the specified proton to the C7, C9 and C16 carbons.
[b] Could not be individually selected in a 1D NOESY experiment due to signal overlap; the NOE correlations could be detected and assigned by selecting the correlation partner instead.
[c] Not detected due to exchange broadening of the proton peak.

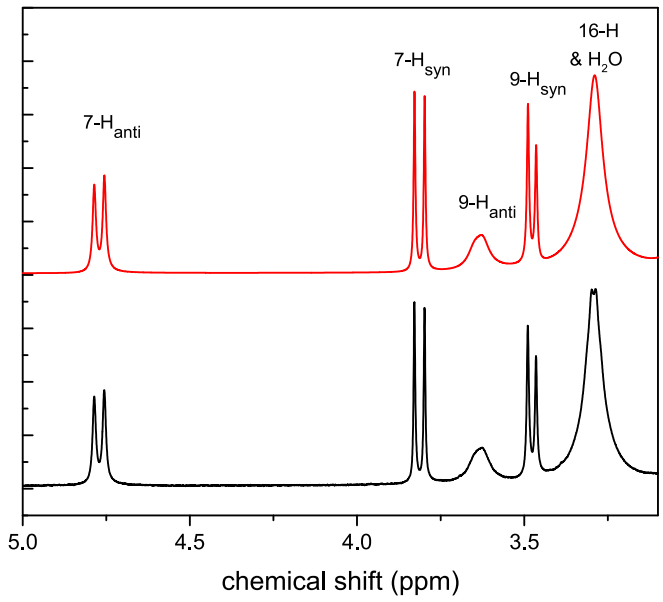

Fig. 4. The 5.0–3.1 ppm region of the ^{1}H NMR spectrum of complex **2** in DMSO-d_6 solution at 303 K. Black: observed, red: simulated with dynamic lineshape fitting, assuming fast-intermediate exchange between the conformers A and B with *pop*(A) = 90%, *k*(forward) = 1250 s^{-1} and $\Delta\delta^{sim}$-values between the two limiting conformers as given in Table 2. The overlapping 16-H & H_2O peak was not included in the simulation and was modelled with a single broad line.

standard 2D NMR correlation spectroscopy (COSY, NOESY, HSQC, HMBC) and the full list of assigned ^{1}H and ^{13}C chemical shifts is given in the Experimental section. The geminal hydrogens at C7 and C9 are denoted by "syn" if they are on the same side of their ring as the L-alanine bridge, and by "anti" otherwise (cf. Figs. 1 and 2). The presence of a chiral carbon (C16) in the ligand makes its two phenolate arms chemically inequivalent in both *cis* and *trans* isomer, and thus these arms display distinct ^{1}H and ^{13}C chemical shifts. The carbons of the phenolate arm on the side of the 16-H hydrogen are numbered as C1–C7 whereas those on the 16-Me side are numbered as C9–C15.

The coordination geometry at the central Mo atom as well as the preferred solution conformation of *cis*-**1** and *trans*-**1** were deduced mainly from.

1) the observed ^{1}H–^{1}H NOE correlations (indicating spatial proximity between the correlated protons)
2) the chemical shift values of the 7-H and 9-H protons (as protons close to the Cl ligand become deshielded)
3) the three-bond ^{1}H–^{13}C correlations seen in the HMBC spectra optimized for 10 Hz long-range couplings (the strongest correlations are expected for such H–X–Y–C coupling pathways where the H–X and Y–C bonds are anti-periplanar about the X–Y bond).

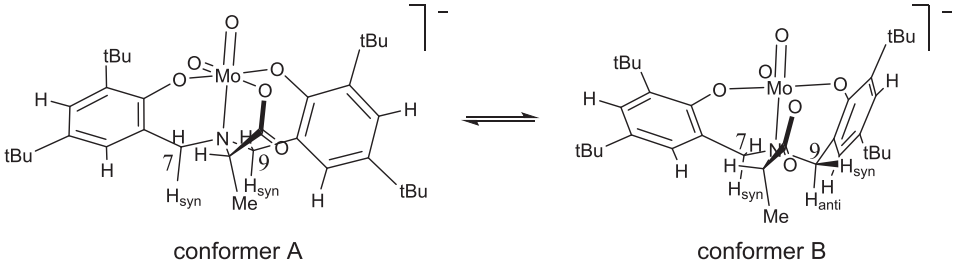

Fig. 3. The predominant solution conformers A (major) and B (minor) of the complex anion (*trans*-**2**) as obtained from MM conformational search followed by DFT geometry optimization.

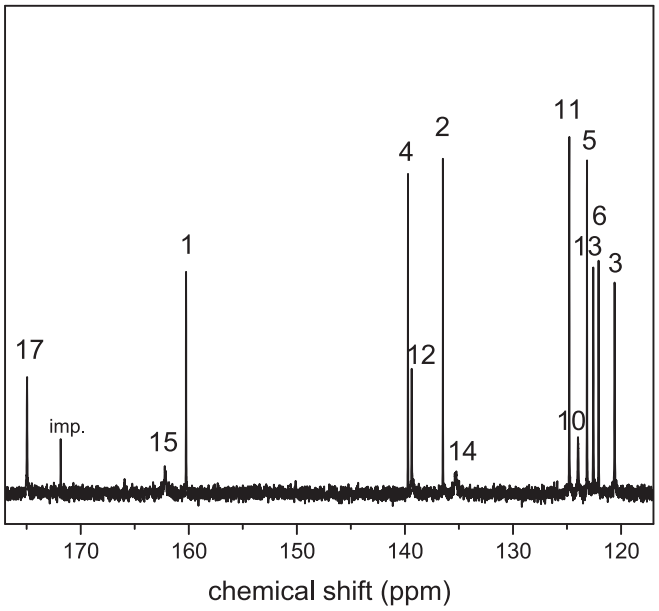

Fig. 5. The aromatic region of the ^{13}C NMR spectrum of complex **2** in DMSO-d_6 solution at 303 K, showing exchange broadening of many of the carbon peaks. The peak assignment follows our numbering for the carbons (cf. e.g. Fig. 3).

A selected set of these data are summarized in Table 1. The solution structures shown in Figs. 1 and 2 for *cis*-**1** and *trans*-**1**, respectively, were obtained from molecular-mechanics (MM2) geometry optimizations of starting structures that were hand-built to satisfy the above-mentioned NMR spectroscopic geometry constraints. The optimized structures agree well with all the observed NMR parameters. For example, in *cis*-**1** the chemical shift of 7-H$_{syn}$ (4.79 ppm) is strongly deshielded by the Cl ligand compared with 7-H$_{anti}$ (3.73 ppm), and a strong NOE correlation between 7-H$_{syn}$ and 16-H can be seen, as well as a HMBC correlation between 7-H$_{syn}$ and C9 (indicating their anti-periplanar positions about the C7–N8 bond). It is thus concluded that in *cis*-**1** and *trans*-**1** the phenolate oxygens are *cis* and *trans* coordinated, respectively, to the central Mo atom and that in $CDCl_3$ solution these complexes adopt a single predominant conformation as shown in Figs. 1 and 2. These conformers are almost identical with the corresponding solid-state (X-ray) structures discussed later.

The dioxo product **2** was poorly soluble in chloroform and was dissolved in DMSO-d_6 for NMR measurements. In the ^{1}H and ^{13}C NMR spectra, the peaks of both the diamagnetic, monomeric complex anion **2** and a triethylammonium cation were seen, with ca. 1:1 M ratio of the ions. Thus, the synthesis of complex **2** as described above yields **2** as its triethylammonium salt $(Et_3NH)[MoO_2(L^{ala})]$. The full list of assigned chemical shifts is given in the Experimental section. Exchange broadening (denoted here with "br") was clearly visible in many of the ^{1}H and ^{13}C NMR peaks of anion **2** at 30 °C (cf. Figs. 4 and 5), *i.e.* the anion in solution undergoes some dynamic process(es) whose rate is within the "fast–intermediate" exchange regime on the NMR time scale.

In order to elucidate the nature of the exchange process of anion **2**, computational conformational search followed by geometry optimization and ^{1}H/^{13}C NMR chemical shift calculation was employed (cf. Experimental for details). Both *cis*- and *trans*-geometries of the complex anion were modelled, but only the *trans*-geometry produced computational results consistent with the observed NMR spectra. Thus, it is concluded that the dioxo product **2** is the *trans*-**2** isomer, as shown in Scheme 1. Two low-energy conformers were found for *trans*-**2** by molecular-mechanics conformational search, and their geometries were further optimized at B3LYP/def2-TZVP level of theory to yield conformer A (ref. 0 kJ/mol) and B (+4.6 kJ/mol in gas-phase and + 5.5 kJ/mol in DMSO, using PCM solvent model). The conformers *trans*-**2**-A and *trans*-**2**-B are shown in Fig. 3. The structure of the major conformer A closely resembles the structure of *trans*-**1**. *Trans*-**2**-B, the higher-energy conformer, has a computational Boltzmann factor of ca. 0.11 relative to A at 30 °C in DMSO solution. Its C9-carrying ring adopts a conformation clearly different from that in conformer A. As a result, e.g. the 9-H$_{syn}$ bond in B adopts a *syn*-clinal position relative to the Mo–N8 bond, in contrast with the anti-periplanar position in A. This conformational change is accompanied with the benzene ring attached to C9 turning away from the L-alanine arm, so that the overall ligand geometry becomes more bent than in A. We postulate the observed exchange broadening in some of the ^{1}H and ^{13}C NMR spectral peaks of **2** to be caused by the interconversion of conformers A and B. This was supported by chemical shift calculations for these conformers together with dynamic NMR lineshape analyses of the experimental NMR spectra, as described below.

Table 2
Selected calculated ^{1}H and ^{13}C chemical shifts δ^{calc} (ppm) of the limiting conformers A and B, $\Delta\delta^{calc} = \delta^{calc}(A) - \delta^{calc}(B)$ and the corresponding $\Delta\delta^{sim}$ from dynamic lineshape fitting to observed NMR spectra, and the experimental dynamically averaged chemical shifts δ^{obs} for (*trans*-) **2**.

nucleus	δ^{calc}(A)/ppm	δ^{calc}(B)/ppm	$\Delta\delta^{calc}$	$\Delta\delta^{sim}$	δ^{obs}/ppm
7-H$_{anti}$	5.35	5.26	0.09	0.45	4.77
7-H$_{syn}$	3.88	3.82	0.06	0.27	3.81
9-H$_{anti}$	4.20	3.36	0.84	1.00	3.63 (br)
9-H$_{syn}$	3.66	3.68	−0.02	−0.33	3.48
16-H	3.49	3.74	−0.25	–	3.29
C1	160.61	161.93	−1.32		160.3
C2	135.90	136.82	−0.92		136.5
C3	122.38	122.18	0.20		120.6
C4	139.45	140.25	−0.80		139.7
C5	122.41	121.67	0.74		123.2
C6	122.76	123.13	−0.37		122.1
C10	124.70	125.95	−1.25		124.0 (br)
C11	122.32	123.52	−1.20		124.8
C12	140.02	140.31	−0.29		139.4 (br)
C13	123.88	123.70	0.18		122.6
C14	138.25	133.78	4.47		135.4 (br)
C15	161.23	165.11	−3.88		162.2 (br)
C17	175.46	177.74	−2.28		174.9 (br)

The ^{1}H and ^{13}C isotropic shielding constants σ_{iso} were calculated for conformers A and B of *trans*-**2** by using the GIAO method (cf. Experimental). Since the oxochloro complexes *cis*-**1** and *trans*-**1** displayed near-uniform solution conformations they were convenient reference compounds for calibration of the computational method. Thus, the shielding constants were calculated also for the DFT optimized structures of *cis*-**1** and *trans*-**1** and their observed chemical shifts were fitted to the calculated shielding constants, yielding the following linear regression equations:

$$\delta_H = -0.95293\cdot\sigma_{iso} + 30.44383 \quad (N = 16,\ r = 0.998,\ RSS = 0.16)$$

$$\delta_C = -1.03768\cdot\sigma_{iso} + 196.4006 \quad (N = 34,\ r = 0.9996,\ RSS = 49.8)$$

These equations were then used to convert the calculated σ_{iso} values for *trans*-**2**-A and -B to chemical shifts δ^{calc} (Table 2).

According to the calculated ^{1}H chemical shifts, there is a large difference between the 9-H$_{anti}$ proton shifts in the limiting conformers A and B ($\Delta\delta^{calc} = 0.84$ ppm). This can be explained by deshielding effect of the adjacent Mo = O bond on 9-H$_{anti}$ in conformer A. This is exactly the proton that shows considerable exchange broadening in the experimental ^{1}H NMR spectrum of complex **2** (cf. Fig. 4). For the carbon nuclei, the largest $\Delta\delta^{calc}$ were calculated for C7 (3.85 ppm), C14 (4.47 ppm), C15 (–3.88 ppm), C16 (–2.80 ppm), and C17 (–2.28 ppm). Consistently, all these carbons displayed broad lineshapes in the experimental ^{13}C NMR spectrum of **2** (cf. Fig. 5). While in DMSO-d_6 solution (m.p. 19 °C) it was not possible to lower the temperature sufficiently to freeze out the individual NMR spectra of the limiting conformers, and only their dynamical average was experimentally observed, the good correlation

Table 3
Summary of crystallographic data for *cis*-**1** and *trans*-**1**.

	cis-**1**	*trans*-**1**
Formula	$C_{37}H_{54}ClMoN_3O_5$	$C_{33}H_{48}ClMoNO_5$
CCDC number	2,241,830	2,241,831
Crystal system	Monoclinic	Monoclinic
Space group	$P2_1$	$P2_1$
a/Å	11.8644(3)	13.8290(3)
b/Å	11.1198(2)	16.6221(4)
c/Å	14.5986(3)	14.7935(3)
β/°	97.253(2)	90.9678(19)
V/Å^3	1910.60(7)	3400.06(14)
Z	2	4
μ(Mo-K$_\alpha$)/cm^{-1}	3.794	4.180
ρ_{calc} g/cm^3	1.308	1.309
2Θ range/°	7.512 to 153.908	8.002 to 139.914
Independent reflections	7932	12,183
R_{int}	0. 0345	0.0297
Parameters	468	796
R_1	0.0223[a] (0.0230)[b]	0.0281[a] (0.0303)[b]
wR_2	0.0548[a] (0.0553)[b]	0.0702[a] (0.0719)[b]
GoF (F^2)	1.035	1.042
Peak, hole/e Å^{-3}	0.23/-0.55	0.63/-0.61
Flack parameter	−0.022(3)	−0.025(7)

[a] $I \geq 2\sigma(I)$.
[b] For all data.

between $\Delta\delta^{calc}$ and the observed exchange broadening of ^{1}H and ^{13}C NMR peaks strongly supports the postulated conformational equilibrium for complex **2** in solution. Some observed HMBC correlations are also nicely in agreement with the presence of minor conformer B (cf. Table 1). For example, a HMBC correlation peak between 9-H$_{syn}$ and C7 is expected to be weak or missing in a structure like conformer *trans*-**2**-A due to unfavorable H$_{syn}$–C9–N8–C7 dihedral angle: this correlation was, indeed, *not* observed for the analogous structure *trans*-**1**. Yet, this correlation peak was observed in the HMBC spectrum of complex **2**, and can be explained with the favorable anti-periplanar relation between the 9-H$_{syn}$ and N8–C7 bonds in the minor conformer B.

Finally, dynamic lineshape fitting and simulation was performed for selected regions of the exchange-broadened ^{1}H and ^{13}C NMR spectra of complex **2**. Based on the calculated Boltzmann factor of 0.11 for B, the population of conformer A was set at 90% and that of B at 10% in this simulation. The calculated chemical shift differences guided the initial guess of these values in the simulation. An example of a dynamic ^{1}H lineshape simulation is shown in Fig. 4 for the geminal protons at C7 and C9. From the lineshape analysis of NMR spectra in a fast-intermediate exchange regime (*i.e.* when a single, averaged spectrum is observed) it is very difficult or impossible to obtain precise rate constants k due to interdependence of the various fitting parameters (populations, chemical shifts of the limiting forms, rate constants). An approximate value $k = 1250$ s^{-1} (303 K) was obtained from this example simulation for the forward rate constant of conformational change A → B, when using the aforementioned populations and reasonable $\Delta\delta^{sim}$ values (cf. Table 2) in the simulation. This should be regarded as an order-of-magnitude estimate; the corresponding ^{13}C lineshape analyses tended to converge to k-values approximately one half of the above value.

In summary, the observed exchange broadening in the ^{1}H and ^{13}C NMR solution spectra of **2** can be explained very well by the postulated fast-intermediate conformational equilibrium process between conformers A and B. The dynamic NMR simulations based on this hypothesis and computational data produce results that are in good agreement with the observed NMR spectra.

3.3. Solid-state structures.

Crystals of *cis*-**1** and *trans*-**1** were obtained from acetonitrile and their solid-state structures were verified by single crystal X-ray diffraction (Table 3). *Cis*-**1** crystallised with two molecules of acetonitrile in the asymmetric unit whereas there are two complex units in the asymmetric unit of *trans*-**1**, respectively. As suggested by the NMR data (see above), both isomers form monomeric molecules in which the L-alanine bisphenolate group has coordinated as a tetradentate trianionic ligand through three oxygen donors and one nitrogen donor (Figs. 6 and 7, Table 4). In both compounds, the nitrogen donor is located trans to the terminal oxido ligand while the Mo–N bonds are relatively long due to the strong structural *trans* effect of multiple bonded oxido ligands [29]. As expected, the coordination sphere around the Mo(VI) is very similar to those found earlier for *trans*-MoOCl(L^{gly}) (L^{gly} = tetradentate glycine

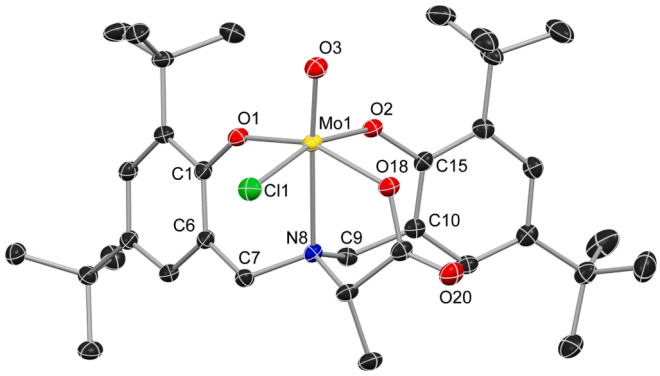

Fig. 6. The molecular structure of *cis*-**1**. Solvent molecules and hydrogen atoms are omitted for clarity. Displacement ellipsoids are presented at the 50% probability level.

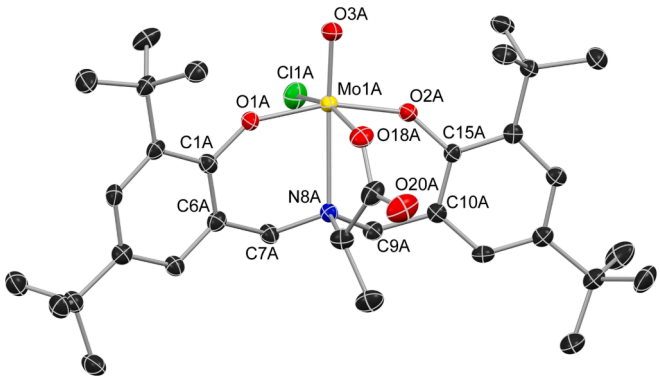

Fig. 7. The molecular structure of *trans*-**1**. Only one of two distinct molecules in the asymmetric unit is shown. Hydrogen atoms are omitted for clarity. Displacement ellipsoids are presented at the 50% probability level.

Table 4
Selected bond lengths [Å] and angles [°] for *cis*- **1**, *trans*-**1** and *trans*-MoOCl(L^{gly}).

	cis-**1**	*trans*-**1**[a]	*trans*-MoOCl(L^{gly})[b]
Mo1-O1	1.8719(19)	1.878(4)	1.8724(14)
Mo1-O2	1.910(2)	1.875(3)	1.8811(14)
Mo1-O3	1.682(2)	1.677(3)	1.6766(15)
Mo1-O18	1.985(2)	2.012(2)	2.0149(14)
Mo1-N8	2.398(2)	2.428(3)	2.4266(17)
Mo1-Cl1	2.3696(7)	2.3446(8)	2.3513(5)
O3-Mo1-N8	175.00(9)	168.29(14)	168.80(7)
O1-Mo1-O2	93.93(8)	162.38(13)	162.11(6)
O1-Mo1-O18	155.69(8)	90.53(15)	86.58(6)
O18-Mo1-Cl1	85.89(6)	162.56(8)	162.15(4)
Mo1-O1-C1	142.47(17)	146.5(3)	141.50(13)
Mo1-O2-C15	134.94(17)	143.4(3)	142.33(13)
Mo1-O18-C17	125.38(19)	127.2(2)	128.17(13)
N8-C16-C17-O18	32.9(3)	25.9(6)	2.3(3)

[a] For one of two similar molecules in the asymmetric unit.
[b] From reference [14].

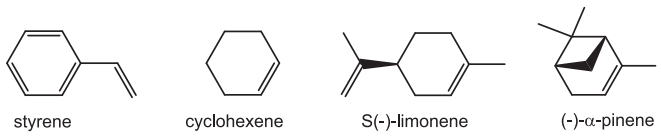

Fig. 8. Substrates used for the catalytic oxidation studies.

bisphenol), *cis/trans*-MoCl(L^{ae}) (L^{ae} = tetradentate aminoethanol bisphenol) and MoOCl(L^{tris}) (L^{tris} = amine trisphenol) [13,15,30,31]. In both *cis* and *trans* isomers, the bonding parameters between the metal centre and the trianionic amino carboxylate bisphenolate ligand are in accordance with the previous studies on oxidomolybdenum(VI) complexes with tripodal aminoalcohol bisphenolates and amine trisphenolates.

Unlike the two isomers of **1**, we were not successful in obtaining a well-resolved crystal structure of the anionic complex **2** (see ESI for further information). We were, however, able to acquire a preliminary structure (ESI, Figure S1), which matches well with the NMR results demonstrating clearly the formation of the expected trans isomer of **2** in which the two phenolato moieties are in a *trans* arrangement and the two oxido O atoms at *cis* positions relative to each other. The complex is monoanionic as also suggested by the 1:1 ratio of complex anions and triethylammonium cations present in the crystal structure.

3.4. Catalytic oxidation of alkenes

Trans-**1** and **2** were studied in the catalytic epoxidation of alkenes, namely styrene, cyclohexene and their naturally occurring derivatives, *i.e. S*(–)-limonene and (–)-α-pinene (Fig. 8), using 30% aqueous H_2O_2 or *tert*-butyl hydroperoxide (tBuOOH) as oxidants in 1,2-dichloroethane (DCE) solutions. To find appropriate reaction conditions for a maximum conversion of alkenes to epoxides, different reaction parameters were considered, that is the temperature, reaction time, amount of catalyst (0.5, 1, 2 and 3 mol% loadings) and oxidant (1:1, 2:1, 3:1 and 4:1 M ratios to substrate). When the reaction conditions were optimized, 2 mol% of catalysts were considered sufficient to run the oxidations at 80 °C in the 1 h of the reaction time with 3:1 M ratio of oxidant to substrate.

Styrene is generally oxidized by H_2O_2 or tBuOOH as oxidants and metal complexes as catalysts to yield five oxidation products, specifically styrene oxide, benzaldehyde, benzoic acid, phenylacetaldehyde and 1-phenylethane-1,2-diol (Fig. 9). Styrene oxide can be formed in the first step, but very fast further reaction converts the product into benzaldehyde via nucleophilic attack of the oxidant to styrene oxide followed by the cleavage of the intermediate hydroperoxystyrene, which can be also further oxidized to benzoic acid [32]. Besides, the formation of benzaldehyde may also result from a radical mechanism by the direct oxidative cleavage of the styrene side-chain double bond. The partial decomposition of the catalyst and thus the very low conversion of styrene, in case of H_2O_2, can be attributed to the presence of water. Similarly, the presence of water can also bring on the formation of 1-phenylethane-1,2-diol by the hydrolysis of styrene oxide. Finally, phenylacetaldehyde can be formed during the isomerisation of styrene oxide. In our case, the oxidation of styrene leads to the formation of

Table 5
Oxidation of styrene.

Catalyst (amount)	Oxidant	Conversion (%)	Epoxide (%)[a]	Benzaldehyde (%)	Benzoic acid (%)
trans-**1** (1 mol%)	30% H_2O_2	12	31	69	–
trans-**1** (2 mol%)	30% H_2O_2	16	41	59	–
trans-**1** (1 mol%)	tBuOOH	65	25	53	22
trans-**1** (2 mol%)	tBuOOH	94	16	51	33
2 (1 mol %)	30% H_2O_2	11	10	83	7
2 (2 mol %)	30% H_2O_2	28	17	68	15
2 (1 mol %)	tBuOOH	60	30	62	8
2 (2 mol %)	tBuOOH	91	19	71	10

[a] The absolute calibration curve method was used for selectivity determination.

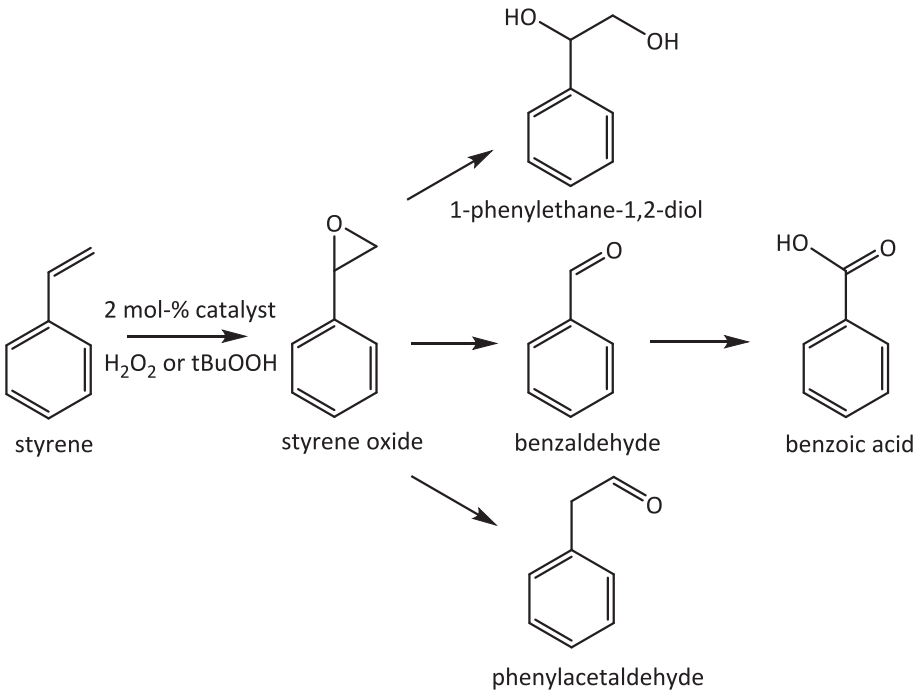

Fig. 9. Various products of catalytic oxidation of styrene.

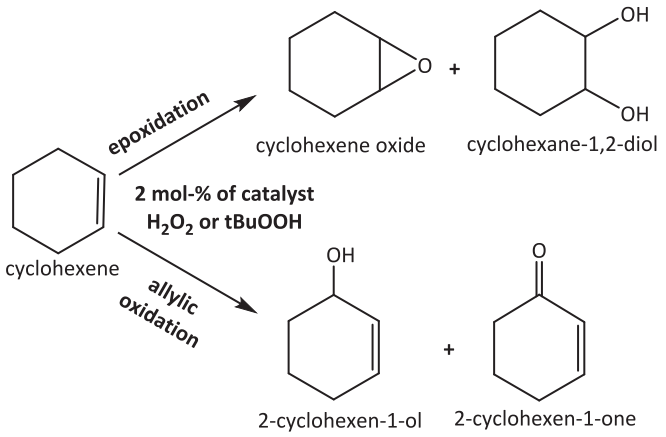

Fig. 10. Various products of catalytic oxidation of cyclohexene.

Table 6
Oxidation of cyclohexene, *S*(–)-limonene and (–)-α-pinene.

Catalyst (amount)	Substrate	Oxidant	Conversion (%)	Epoxide (%)[a]
trans-**1** (2 mol%)	cyclohexene	30% H_2O_2	25	100
trans-**1** (1 mol%)	cyclohexene	tBuOOH	72	94
trans-**1** (2 mol%)	cyclohexene	tBuOOH	99	100
trans-**1** (2 mol%)	*S* (–)-limonene	30% H_2O_2	6	86
trans-**1** (2 mol%)	*S* (–)-limonene	tBuOOH	99	27[b]
trans-**1** (2 mol%)	(–)-α-pinene	30% H_2O_2	5	81
trans-**1** (2 mol%)	(–)-α-pinene	tBuOOH	99	100
2 (2 mol%)	cyclohexene	30% H_2O_2	29	93[c]
2 (1 mol%)	cyclohexene	tBuOOH	63	96
2 (2 mol%)	cyclohexene	tBuOOH	99	99
2 (2 mol%)	*S* (–)-limonene	30% H_2O_2	18	100
2 (2 mol%)	*S* (–)-limonene	tBuOOH	87	100
2 (2 mol%)	(–)-α-pinene	30% H_2O_2	4	76
2 (2 mol%)	(–)-α-pinene	tBuOOH	71	100

[a] The absolute calibration curve method was used for selectivity determination.
[b] Diepoxide was found with selectivity of 65%.
[c] Formation of cyclohex-2-en-1-one as by-product.

benzaldehyde as a major component along with smaller amounts of styrene oxide and benzoic acid (Table 5). The yields of all products were rather low when H_2O_2 was used as an oxidant, but use of tBuOOH lead to high conversions, whereas both catalysts have a rather similar reaction outcome. Formation of benzaldehyde by the oxidative cleavage of the C═C double bond in styrene is frequently seen in epoxidation experiments, thus only a few selective epoxidation catalysts have been reported. [33–35].

Oxidation of cyclohexene generally results in epoxidation products, *i.e.* cyclohexene oxide, and after its hydrolysis to cyclohexene-1,2-diol, or in allylic oxidation products, *i.e.* 2-cyclohexen-1-ol and 2-cyclohexen-1-one (Fig. 10). In this study, the mono- and bicyclic monoterpenes possessing cyclohexene ring, *i.e.* *S*(–)-limonene and (–)-α-pinene also give the corresponding oxidation products. Cyclohexene, *S*(–)-limonene and (–)-α-pinene were oxidized more selectively than styrene with both catalysts while generally the epoxide was the major product (Table 6). Complex *trans*-**1** gave 25% yield but 100% selectivity whereas for complex **2** the conversion of cyclohexene is only slightly higher (29%) giving epoxide in a high selectivity with cyclohex-

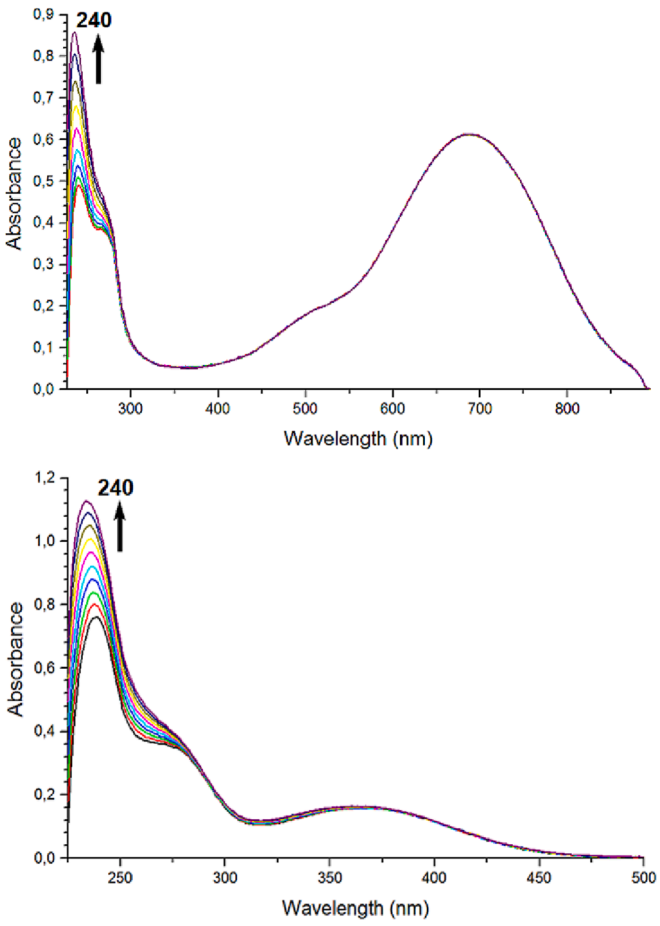

Fig. 11. Spectral changes during titration of (top) 2 ml of a $4.0 \cdot 10^{-5}$ M solution of *trans*-**1** and (bottom) 2 ml of a $4.5 \cdot 10^{-5}$ M solution of **2** catalysts in DCE after successive addition of one-drop portions of aqueous 30% H_2O_2.

2-en-1-one as a minor product when H_2O_2 was used as an oxidant. In case of monoterpenes, the yields are much lower but selectivity is still very high. On the other hand, the use of tBuOOH provided epoxide practically quantitatively with excellent conversions using both catalysts, but including the formation of diepoxide when *trans*-**1** was a catalyst in oxidation of *S*(–)-limonene possessing additionally exocyclic isopropenyl moiety. C*is*- and *trans*-1,2-limonene oxides are formed almost in equal proportions, but when H_2O_2 was used as oxidant the ratio between the *cis/trans* isomers is 1:2. It is also noteworthy that in the oxidation of cyclohexene, *S*(–)-limonene and (–)-α-pinene, in comparison to other molybdenum(VI) complexes (e.g. with Schiff base ligands) [36–38], *trans*-**1** gave in each case much higher conversions and selectivities towards epoxides with 2 mol% loading, excluding oxidation of *S*(–)-limonene. Complex **2** show similar conversions and selectivities for monoterpenes, but in contrast to cyclohexene when much higher 99% conversion was observed. In general, *trans*-**1** seems to be slightly more active and selective as an epoxidation catalyst than dioxido complex **2**.

Studies on monomeric and polymeric dioxidomolybdenum(VI) complexes with pyridoxal thiosemicarbazone ligands also revealed different reactivity between the neutral and charged cationic compounds in the oxidation of cyclooctene by aqueous tBuOOH [39]. Under the solvent-free conditions and with a low catalyst:substrate ratio (1:2000), the monomeric neutral $MoO_2L(MeOH)$ complex is the most efficient catalyst with very good conversion and selectivity (both 97%) after 6 h of reaction time. While similar charged complex $[MoO_2LH(MeOH)]Cl$, with protonated pyridoxal nitrogen, is much less active with 48% conversion and 74% selectivity towards cyclooctene oxide. On the other hand, corresponding charged polymer $\{[MoO_2LH]Cl\}_n$ showed

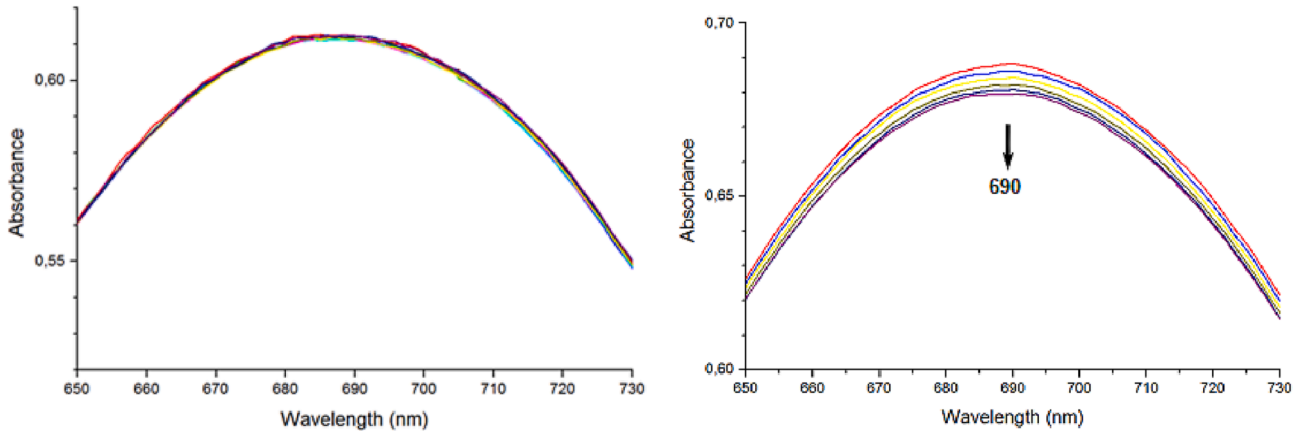

Fig. 12. Spectral changes in the 650–730 nm region during titration of *trans*-**1** after successive addition of one-drop portions of (left) aqueous 30% H_2O_2 and (right) tBuOOH in DCE.

much higher 70% conversion and 82% selectivity. Surprisingly, analogous neutral polymeric dioxidomolybdenum(VI) complex $[MoO_2L]_n$ revealed only 54% conversion, but with similar selectivity towards epoxide.

3.5. Reactivity with hydrogen peroxide and tert-butyl hydroperoxide

A variety of molybdenum(VI) complexes have been found to react with H_2O_2 and tBuOOH to form the corresponding oxidoperoxido complexes. To shed some light on the mechanism of these catalytic reactions and establish the generation of such species, UV–Vis spectroscopy was involved. Spectral changes were monitored by recording a series of spectra after a successive addition of one-drop portions of aqueous 30% H_2O_2 or tBuOOH in decane to the solution of the catalysts *trans*-**1** or **2** in DCE. The UV–Vis spectra presented in Fig. 11, show changes during the titrations of both complexes with H_2O_2, which cause a small shift of the 240 nm band to 235 nm along with considerable increase in the intensities of these strong intraligand π-π* transitions. Titrations with tBuOOH cause similar changes in the spectra in this region, but additional decrease in the 690 nm band can be noticed in comparison to titration made with H_2O_2 Fig. 12. In our opinion, these changes show that interaction of the complexes with tBuOOH is much stronger than H_2O_2 and indicate the plausible formation of the oxidoperoxidomolybdenum(VI) complex, which in the catalytic reaction finally transfers oxygen to an appropriate organic substrate to give epoxidation products. Similar changes have been noticed, *i.e.* considerable increase in intensity of intraligand π-π* and slowly decrease in intensity of charge transfer transitions in various molybdenum(VI) complexes [40,41].

4. Conclusion

The reaction of $[MoO_2Cl_2(dmso)_2]$ with a chiral tetradentate O_3N-type L-alanine bisphenol ligand precursor $(Et_3NH)H_2L^{ala}$ leads to the formation of an oxidochloridomolybdenum(VI) complex $[MoOCl(L^{ala})]$ **1** as two separable geometric isomers. In the major product, *trans*-**1,** the phenolate groups are in *trans* positions**,** whereas in the minor component, *cis*-**1,** the phenolate groups are positioned in *cis* positions. Both complexes crystallize as monomeric molecules, in which the ligand has a tetradentate coordination through three oxygen donors and one nitrogen donor. The reaction of $Na_2MoO_4{\cdot}2H_2O$ with the same ligand in an acidic methanol solution leads to the formation of an anionic dioxido complex $(Et_3NH)[MoO_2(L^{ala})]$ **2** with a *trans* coordination of the tetradentate ligand. *Trans*-**1** and **2** were tested as catalysts for epoxidation styrene, cyclohexene S(–)-limonene and (–)-α-pinene using H_2O_2 and tBuOOH as oxidants. The oxidation of styrene with H_2O_2 using catalyst *trans*-**1** yielded predominantly benzaldehyde while epoxide was formed only as a minor product. Benzaldehyde was the major product also with tBuOOH as an oxidant while styrene oxide and benzoic acid were the minor components. With catalyst **2**, benzaldehyde was formed along with smaller amounts of styrene oxide and benzoic acid. Epoxidation of cyclohexene was selective with both oxidants and other oxidation products, *i.e.* 2-cyclohexen-1-one were seen only as minor quantities when **2** was used as a catalyst. (–)-α-pinene was epoxidized in high yields and selectivities with both catalysts using tBuOOH as an oxidant, while H_2O_2 gave remarkable lower yields. S(–)-limonene was oxidized by H_2O_2 in low yields and high selectivities with both catalysts, however the use of tBuOOH with *trans*-**1** yielded the mixture of mono- and diepoxide in a high conversion.

CRediT authorship contribution statement

Anssi Peuronen: Formal analysis, Methodology, Visualization, Writing – original draft. **Henri Kivelä:** Formal analysis, Methodology, Visualization, Writing – original draft. **Pasi Salonen:** Formal analysis, Methodology. **Ville Eskonen:** Formal analysis, Methodology. **Marta Karman:** Formal analysis, Methodology. **Manu Lahtinen:** Formal analysis, Methodology. **Grzegorz Romanowski:** Supervision, Project administration, Writing – review & editing. **Ari Lehtonen:** Conceptualization, Supervision, Project administration, Writing – original draft, Writing – review & editing.

Declaration of Competing Interest

The authors declare that they have no known competing financial interests or personal relationships that could have appeared to influence the work reported in this paper.

Data availability

Data will be made available on request.

Acknowledgements

AP gratefully acknowledges the financial support by the Academy of Finland (project 315911). HK wishes to acknowledge CSC – IT Center for Science, Finland, for computational resources and access to software, and Petteri Vainikka for helpful discussions.

Appendix A. Supplementary data

Supplementary data to this article can be found online at https://doi.

org/10.1016/j.ica.2023.121519.

References

[1] A.W. Kleij, Nonsymmetrical salen ligands and their complexes: Synthesis and applications, Eur. J. Inorg. Chem. 2009 (2) (2009) 193–205.
[2] G. Licini, M. Mba, C. Zonta, Amine triphenolate complexes: Synthesis, structure and catalytic activity, J. Chem. Soc. Dalt. Trans. (27) (2009) 5265.
[3] O. Santoro, C. Redshaw, Metallocalix[n]arenes in catalysis: A 13-year update, Coord. Chem. Rev. 448 (2021), 214173, https://doi.org/10.1016/j.ccr.2021.214173.
[4] O. Wichmann, R. Sillanpää, A. Lehtonen, Structural properties and applications of multidentate [O, N, O, X'] aminobisphenolate metal complexes, Coord. Chem. Rev. 256 (2012) 371–392, https://doi.org/10.1016/j.ccr.2011.09.007.
[5] R. Hille, R. Mendel, Molybdenum in living systems, Coord. Chem. Rev. 255 (2011) 991–992, https://doi.org/10.1016/j.ccr.2010.10.014.
[6] C. Schulzke, A.C. Ghosh, Molybdenum and Tungsten oxidoreductase models, in: Bioinspired Catal. Met. Complexes, 2014, pp. 349–382, https://doi.org/10.1002/9783527664160.ch13.
[7] K. Most, J. Hoßbach, D. Vidović, J. Magull, N. Mösch-Zanetti, Oxygen-transfer reactions of molybdenum- and tungstendioxo complexes containing η2-pyrazolate ligands, Adv. Synth. Catal. 347 (2-3) (2005) 463–472.
[8] A. Günyar, D. Betz, M. Drees, E. Herdtweck, F.E. Kühn, Highly soluble dichloro, dibromo and dimethyl dioxomolybdenum(VI)- bipyridine complexes as catalysts for the epoxidation of olefins, J. Mol. Catal. A Chem. 331 (1-2) (2010) 117–124.
[9] S. Pätsch, J.V. Correia, B.J. Elvers, M. Steuer, C. Schulzke, Inspired by nature—functional analogues of molybdenum and tungsten-dependent oxidoreductases, Molecules. 27 (12) (2022) 3695.
[10] J.-M. Brégeault, Transition-metal complexes for liquid-phase catalytic oxidation: Some aspects of industrial reactions and of emerging technologies, J. Chem. Soc. Dalt. Trans. (17) (2003) 3289–3302.
[11] S. Shylesh, M. Jia, W.R. Thiel, Recent progress in the heterogenization of complexes for single-site epoxidation catalysis, Eur. J. Inorg. Chem. 2010 (28) (2010) 4395–4410.
[12] S. Mrkonja, E. Topić, M. Mandarić, D. Agustin, J. Pisk, Efficient molybdenum hydrazonato epoxidation catalysts operating under green chemistry conditions: Water vs, decane competition, Catalysts. 11 (2021), https://doi.org/10.3390/catal11070756.
[13] J. Hakala, R. Sillanpää, A. Lehtonen, Oxidomolybdenum(VI) complexes with aminoalcohol bis(phenolate) [O, N, O, O′] ligands: Synthesis and catalytic studies, Inorg. Chem. Commun. 21 (2012) 21–23, https://doi.org/10.1016/j.inoche.2012.03.043.
[14] T. Heikkilä, R. Sillanpää, A. Lehtonen, Oxomolybdenum(VI) complexes with glycine bisphenol [O, N, O, O'] ligand: Synthesis and catalytic studies, J. Coord. Chem. 67 (11) (2014) 1863–1872.
[15] F. Romano, A. Linden, M. Mba, C. Zonta, G. Licini, Molybdenum(VI) amino triphenolate complexes as catalysts for sulfoxidation, epoxidation and haloperoxidation, Adv. Synth. Catal. 352 (2010) 2937–2942, https://doi.org/10.1002/adsc.201000496.
[16] A.K. Yudin (Ed.), Aziridines and Epoxides in Organic Synthesis, Wiley, 2006.
[17] H. Adolfsson, Transition metal-catalyzed epoxidation of alkenes, in: Mod. Oxid. Methods, 2010, pp. 37–84, https://doi.org/10.1002/9783527632039.ch2.
[18] K.A. Joergensen, Transition-metal-catalyzed epoxidations, Chem. Rev. 89 (3) (1989) 431–458.
[19] B.S. Lane, K. Burgess, Metal-catalyzed epoxidations of alkenes with hydrogen peroxide, Chem. Rev. 103 (7) (2003) 2457–2474.
[20] R. Pereira Limberger, A. Mendes Aleixo, A.G. Fett-Neto, A. T. Henriques, Bioconversion of (+)- and (-)-alpha-pinene to (+)- and (-)-verbenone by plant cell cultures of Psychotria brachyceras and Rauvolfia sellowii, Electron. J. Biotechnol. 10 (4) (2007).
[21] W.A. Duetz, H. Bouwmeester, J.B. Beilen, B. Witholt, Biotransformation of limonene by bacteria, fungi, yeasts, and plants, Appl. Microbiol. Biotechnol. 61 (4) (2003) 269–277.
[22] A.C.R. Da Silva, P.M. Lopes, M.M.B. De Azevedo, D.C.M. Costa, C.S. Alviano, D. S. Alviano, Biological activities of α-pinene and β-pinene enantiomers, Molecules. (2012), https://doi.org/10.3390/molecules17066317.
[23] M. Blair, P. Andrews, B. Fraser, C. Forsyth, P. Junk, M. Massi, K. Tuck, Facile methods for the separation of the cis- and trans-diastereomers of limonene 1,2-oxide and convenient routes to diequatorial and diaxial 1,2-diols, Synthesis (Stuttg). 2007 (10) (2007) 1523–1527.
[24] Y. Li, D. Yu, Z. Dai, J. Zhang, Y. Shao, N. Tang, J. Wu, Bulky metallocavitands with a chiral cavity constructed by aluminum and magnesium atrane-likes: enantioselective recognition and separation of racemic alcohols, Dalt. Trans. 44 (2015) 5692–5702, https://doi.org/10.1039/C4DT03848G.
[25] S. Barroso, P. Adão, A.M. Coelho, J.C. Pessoa, A.M. Martins, Pinacol coupling of benzaldehydes mediated by titanium complexes displaying amine bis(phenolate) ligands, J. Mol. Catal. A Chem. 412 (2016) 107–116.
[26] F.J. Arnáiz, R. Aguado, M.R. Pedrosa, A. De Cian, Addition compounds of dichlorodioxomolybdenum(VI) with sulfoxides. Molecular structure of [MoO2Cl2 (Me2SO)2], Inorganica Chim. Acta. 347 (2003) 33–40, https://doi.org/10.1016/S0020-1693(02)01434-2.
[27] M.J. Frisch, G.W. Trucks, H.B. Schlegel, G.E. Scuseria, M. a. Robb, J.R. Cheeseman, G. Scalmani, V. Barone, G. a. Petersson, H. Nakatsuji, X. Li, M. Caricato, a. V. Marenich, J. Bloino, B.G. Janesko, R. Gomperts, B. Mennucci, H.P. Hratchian, J. V. Ortiz, a. F. Izmaylov, J.L. Sonnenberg, Williams, F. Ding, F. Lipparini, F. Egidi, J. Goings, B. Peng, A. Petrone, T. Henderson, D. Ranasinghe, V.G. Zakrzewski, J. Gao, N. Rega, G. Zheng, W. Liang, M. Hada, M. Ehara, K. Toyota, R. Fukuda, J. Hasegawa, M. Ishida, T. Nakajima, Y. Honda, O. Kitao, H. Nakai, T. Vreven, K. Throssell, J. a. Montgomery Jr., J.E. Peralta, F. Ogliaro, M.J. Bearpark, J.J. Heyd, E.N. Brothers, K.N. Kudin, V.N. Staroverov, T. a. Keith, R. Kobayashi, J. Normand, K. Raghavachari, a. P. Rendell, J.C. Burant, S.S. Iyengar, J. Tomasi, M. Cossi, J.M. Millam, M. Klene, C. Adamo, R. Cammi, J.W. Ochterski, R.L. Martin, K. Morokuma, O. Farkas, J.B. Foresman, D.J. Fox, G16_C01, (2016) Gaussian 16, Revision C.01, Gaussian, Inc., Wallin.
[28] A. Peuronen, R. Sillanpää, A. Lehtonen, The Syntheses and Vibrational Spectra of 16O- and 18O-Enriched cis-MO2(M=Mo, W) Complexes, ChemistrySelect. 3 (13) (2018) 3814–3818.
[29] B.J. Coe, S.J. Glenwright, Trans-effects in octahedral transition metal complexes, Coord. Chem. Rev. 203 (1) (2000) 5–80.
[30] E. Laurén, H. Kivelä, M. Hänninen, A. Lehtonen, Oxidomolybdenum(VI) complexes with atrane-type [O3N] ligands, Polyhedron. 28 (18) (2009) 4051–4055.
[31] A. Lehtonen, R. Sillanpää, Alkoxo, chlorido, and methyl derivatives of oxidomolybdenum(VI) complexes with tetradentate [O3N]-type ligands, Polyhedron. 26 (2007) 5293–5300, https://doi.org/10.1016/j.poly.2007.07.036.
[32] V. Hulea, E. Dumitriu, Styrene oxidation with H2O2 over Ti-containing molecular sieves with MFI, BEA and MCM-41 topologies, Appl. Catal. A Gen. 277 (1-2) (2004) 99–106.
[33] K. Kaneda, K. Morimoto, T. Imanaka, MoO 2 (acac) 2 Complex as a Reagent for Oxidative Cleavage of vic-Diols, Chem. Lett. 17 (8) (1988) 1295–1296.
[34] M.E. Judmaier, A. Wallner, G.N. Stipicic, K. Kirchner, J. Baumgartner, F. Belaj, N. C. Mösch-Zanetti, Molybdenum(VI) dioxo complexes with tridentate phenolate ligands, Inorg. Chem. 48 (2009) 10211–10221, https://doi.org/10.1021/ic901201s.
[35] J.A. Schachner, P. Traar, C. Sala, M. Melcher, B.N. Harum, A.F. Sax, M. Volpe, F. Belaj, N.C. Mösch-Zanetti, Dioxomolybdenum(VI) complexes with pyrazole based aryloxide ligands: Synthesis, characterization and application in epoxidation of olefins, Inorg. Chem. 51 (2012) 7642–7649, https://doi.org/10.1021/ic300648p.
[36] M. Karman, G. Romanowski, Cis-dioxidomolybdenum(VI) complexes with chiral tetradentate Schiff bases: Synthesis, spectroscopic characterization and catalytic activity in sulfoxidation and epoxidation, Inorganica Chim. Acta. 511 (2020), 119832, https://doi.org/10.1016/J.ICA.2020.119832.
[37] M. Karman, G. Romanowski, Synthesis, spectroscopic characterization and catalytic activity of cis -dioxidomolybdenum (VI) complexes with chiral tetradentate Schiff bases, Appl Organomet Chem 34 (12) (2020).
[38] M. Karman, M. Wera, G. Romanowski, Chiral cis-dioxidomolybdenum(VI) complexes with Schiff bases possessing two alkoxide groups: Synthesis, structure, spectroscopic studies and their catalytic activity in sulfoxidation and epoxidation, Polyhedron. 187 (2020), 114653, https://doi.org/10.1016/J.POLY.2020.114653.
[39] J. Pisk, B. Prugovečki, D. Matković-Čalogović, R. Poli, D. Agustin, V. Vrdoljak, Charged dioxomolybdenum(VI) complexes with pyridoxal thiosemicarbazone ligands as molybdenum(V) precursors in oxygen atom transfer process and epoxidation (pre)catalysts, Polyhedron. 33 (2012) 441–449, https://doi.org/10.1016/J.POLY.2011.12.003.
[40] M.R. Maurya, S. Dhaka, F. Avecilla, Synthesis, characterization and catalytic activity of dioxidomolybdenum(VI) complexes of tribasic pentadentate ligands, Polyhedron. 67 (2014) 145–159, https://doi.org/10.1016/J.POLY.2013.08.050.
[41] G. Romanowski, J. Kira, Synthesis, characterization and catalytic activity of dioxidomolybdenum(VI) complexes with tridentate Schiff bases derived from 1R,2S(−)-norephedrine, Polyhedron. 134 (2017) 50–58, https://doi.org/10.1016/J.POLY.2017.06.005.